Radiology

Endovascular Repair of Abdominal Aortic Aneurysm:
Follow-up with Noninvasive Vascular Elastography in a Canine Model[1]

Eli Salloum, MSc
Antony Bertrand-Grenier, Eng, MSc
Sophie Lerouge, PhD
Claude Kauffman, PhD
Hélène Héon, DVM
Eric Therasse, MD
Igor Salazkin, MD
Marie-Hélène Roy Cardinal, PhD
Guy Cloutier, PhD
Gilles Soulez, MD, MSc

Purpose: To assess the ability of noninvasive vascular elastography (NIVE) to help characterize endoleaks and thrombus organization in a canine model of abdominal aortic aneurysm after endovascular aneurysm repair with stent-grafts, in comparison with computed tomography (CT) and pathologic examination findings.

Materials and Methods: All protocols were approved by the Animal Care Committee in accordance with the guidelines of the Canadian Council of Animal Care. Stent-grafts were implanted in a group of 18 dogs with aneurysms created in the abdominal aorta. Type I endoleak was created in four aneurysms; type II endoleak, in 13 aneurysms; and no endoleak, in one aneurysm. Doppler ultrasonography and NIVE examinations were performed at baseline and at 1-week, 1-month, 3-month, and 6-month follow-up. Angiography, CT, and macroscopic tissue examination were performed at sacrifice. Strain values were computed by using the Lagrangian speckle model estimator. Areas of endoleak, solid organized thrombus, and fresh thrombus were identified and segmented by comparing the results of CT and macroscopic tissue examination. Strain values were compared by using the Wilcoxon rank-sum and Kruskal-Wallis tests.

Results: All stent-grafts were successfully deployed, and endoleaks were clearly depicted in the last follow-up elastography examinations. Maximal axial strains over consecutive heart cycles in endoleak, organized thrombus, and fresh thrombus areas were 0.78% ± 0.22, 0.23% ± 0.02, 0.10% ± 0.04, respectively. Strain values were significantly different between endoleak and organized or fresh thrombus areas ($P < .000$) and between organized and fresh thrombus areas ($P < .0002$). No correlation was found between strain values and type of endoleak, sac pressure, endoleak size, and aneurysm size.

Conclusion: NIVE may be able to help characterize endoleak and thrombus organization, regardless of the size, pressure, and type of endoleak.

© RSNA, 2015

© RSNA, 2015

Endovascular aneurysm repair (EVAR) with stent-grafts is a promising alternative to surgery, with lower perioperative mortality and morbidity rates and shorter hospitalization times (1–4). The main limitation of this method is, however, the durability of the aneurysm exclusion and the occurrence of endoleaks, so this repair requires regular follow-up imaging (5). For EVAR surveillance, different modalities, such as computed tomographic (CT) scanning, Doppler ultrasonography (US), contrast material–enhanced US, and magnetic resonance (MR) imaging, have been utilized (6,7). CT is considered the reference standard for follow-up after EVAR but leads to increased costs and exposure to ionizing radiation and contrast agents (8). Furthermore, approximately 65% of follow-up costs have been attributed to CT scanning (9). Therefore, an effort has been made for Doppler US to replace CT (or MR imaging), but the main concern is the lower sensitivity and specificity of the former method in the detection of endoleaks (failure in up to 32% of cases) (10–15).

Noninvasive vascular elastography (NIVE) with the Lagrangian speckle model estimator (LSME) measures the deformation induced by natural cardiac pulsation (16–18). Thus, to generate the elastogram, there is no need to use a low-frequency radiation force, as with the acoustic radiation force impulse imaging technique, or a supersonic shear wave, as with supersonic imaging techniques. NIVE was first developed to help characterize carotid atherosclerotic lesions (19). Then, a study performed by Fromageau et al

(20) reported preliminary data with the LSME in a type I endoleak canine aneurysm model. In the latter study, it was possible to characterize the axial strain of the aneurysm wall and to differentiate the venous patch used to create the model from the native artery, as well as to detect endoleaks as areas of strain decorrelation (equivalent to aliasing at Doppler US). However, our study was limited by its small sample size, the absence of CT examinations as a reference standard for endoleak diagnosis, and the absence of correlation with thrombus organization.

Strain measurement with NIVE thus has the potential of being a complementary follow-up imaging technique to EVAR for detecting endoleaks and characterizing thrombus organization on the basis of its mechanical properties. The purpose of our study was to assess the ability of NIVE to help characterize endoleaks and thrombus organization in a canine model of abdominal aortic aneurysm (AAA) after EVAR with stent-grafts, in comparison with CT and pathologic examination findings.

Materials and Methods

Aneurysm Creation in a Canine Model

All protocols used in our study were approved by the Animal Care Committee in accordance with the guidelines of the Canadian Council of Animal Care. To test NIVE for the detection of endoleaks and the characterization of thrombi within the covered aneurysm sac, AAAs were created in 18 mongrel dogs (all females, 28–40 kg and 6–9 years old). The surgical construction of aneurysms was performed by a vascular surgeon (I.S.) with a jugular vein patch sutured at the anterior portion of the abdominal aorta (21). To create a type

I endoleak, stent-grafts were inserted with a short landing zone and preservation of the collateral vessel patency (collateral flow) (Fig 1a). For a type II endoleak, stent-grafts were implanted with an adequate landing zone and preservation of collateral flow (Fig 1b, 1c). Finally, to obtain a complete seal, stent-grafts were implanted with an adequate landing zone after ligation of all collateral vessels arising from the sac (without collateral flow) (21,22). Stent-grafts (TFLE-Zenith Flex AAA Endovascular Grafts [Cook Medical, Bloomington, Ind] in three dogs and ZFLE-Zenith Flex AAA Endovascular Grafts [Cook Medical] in 15 dogs) were implanted after a recovery period of 8 weeks. All endovascular procedures were performed by a vascular radiologist (G.S., with 22 years of experience). The animals were divided into three groups: Five dogs had a short landing zone (<10 mm) and collateral flow, seven dogs had an adequate landing zone (>15 mm) and collateral flow, and six dogs had an adequate landing zone and ligated collateral arteries. After a period of 6 months, each dog was sacrificed, and a necropsy was performed. The aneurysms were collected and fixed in buffered formalin.

Advances in Knowledge

- US noninvasive vascular elastography (NIVE) may have the potential of being a complementary follow-up imaging technique for the detection of endoleaks after endovascular aneurysm repair (EVAR).
- NIVE was capable of characterizing fresh and organized thrombi on the basis of their mechanical properties ($P < .01$).

Implication for Patient Care

- NIVE could reduce the need for CT angiography, the cost, and the exposure to ionizing radiation and contrast agents involved in the follow-up of abdominal aortic aneurysms after EVAR.

Figure 1: **(a)** Curved planar reformation of AAA after EVAR with a short landing zone at the distal end of the aneurysm shows a type Ib endoleak (arrow). **(b)** Volume-rendered reformation o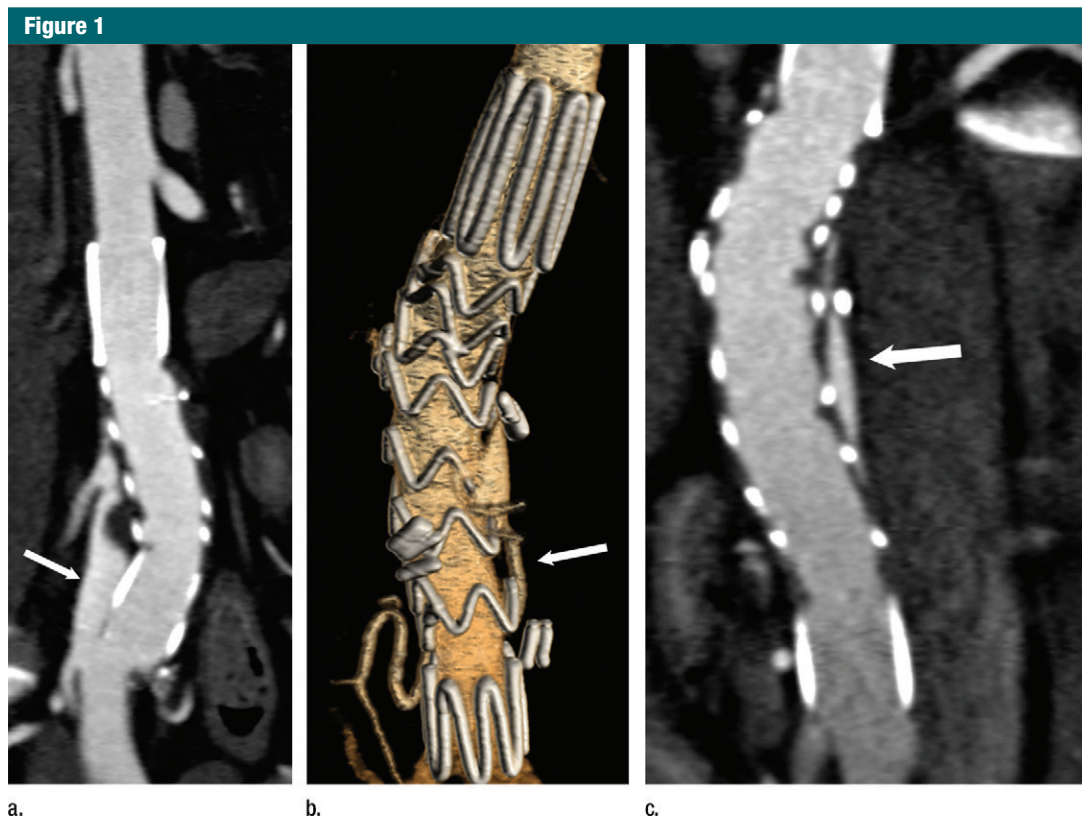f AAA after EVAR shows a type II endoleak fed by the inferior mesenteric artery (arrow). **(c)** Curved planar reformation of the same AAA as in **b** shows the type II endoleak (arrow).

Imaging Protocols

Doppler US and elastography examinations were performed at baseline and at 1-week, 1-month, 3-month, and 6-month follow-up to evaluate the presence, type, and evolution of endoleaks. Angiography and CT were also performed at 6 months, followed by macroscopic tissue cuts after the animals were sacrificed. All acquisitions were performed with the animals receiving general anesthesia and by a technologist with 20 years of experience who was supervised by the same vascular radiologist (G.S.). Before sacrifice but after dissection of the abdomen, the pressure in the aneurysm sac and the aorta was measured by introducing a spinal needle (22 gauge × 3½ inches) (Terumo, Tokyo, Japan) inside the aneurysm sac and the aorta and connecting it to a pressure sensor. Between baseline and sacrifice, measurements of the aneurysm's length, maximum and minimum diameters of the aneurysm, and areas of

the stent-graft and aneurysm were obtained during Doppler US to correlate them with strain parameters and to study the size evolution in the presence and absence of endoleak.

Doppler US.—All external Doppler US examinations were performed by using a US scanner (Supersonic Imagine; Aixplorer, Aix-en-Provence, France) equipped with a 256-element (Super-Linear SL15–4) 7.5-MHz linear-array transducer (pulse repetition frequency, 1.95 kHz; scale, 10 cm/sec; sound speed, 1540 m/sec). The high-definition frame rate was set to middle, the wall filter was set to low, and the smoothing was set to 0. US sequences were performed in longitudinal and three axial planes (eg, in the proximal, middle, and distal parts of the aneurysm).

RF acquisitions.—US radiofrequency (RF) data were acquired by using a Sonix Touch scanner (Ultrasonix, Vancouver, British Columbia, Canada)

equipped with a 128-element L14–5/38 10-MHz linear-array transducer. This probe has a 60% bandwidth at a frame rate of 25 Hz. RF data were sampled at 40 MHz, and acquisitions were performed over approximately 5 seconds for each plane. Systemic pressures and pulse rates were measured at the beginning, middle, and end of the RF acquisitions (LifeWindow 6000 V), as these variables potentially affect strain measures. The acquisitions were performed in the same planes used at Doppler US.

Angiography.—Digital subtraction angiography (Koordinat 3D; Siemens Medical Solutions, Forchheim, Germany) was performed at baseline, before and during implantation of the stent-graft, and at sacrifice by the same interventional radiologist (G.S.). A pigtail catheter (4 or 5 F) was inserted in the abdominal aorta. Acquisitions were performed during the injection
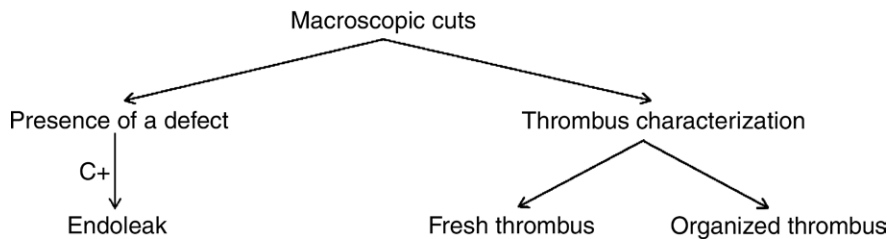
Figure 2

Figure 2: The macroscopic tissue slide is first analyzed to detect the presence of an endoleak through a defect or gap in the aneurysm sac. If the presence of the defect correlates with contrast enhancement at CT *(C+)* in the same region, presence of an endoleak is confirmed. The rest of the tissue in the aneurysmal sac is characterized as organized or fresh thrombus according to its appearance in macroscopic cuts.

of 20 mL (at 10 mL/sec) of an iodinated contrast agent (iopamidol, Isovue 200, Bracco Imaging Canada, Anjou, Quebec, Canada during implantation and Conray 60, Mallinckrodt Canada, Pointe-Claire, Quebec, Canada during sacrifice) at the level of the renal artery and at the distal portion of the aorta to detect type I and II endoleaks.

CT studies.—At sacrifice, a contrast-enhanced CT study (Somatom 64; Siemens Medical Solutions, Erlangen, Germany) was performed before and after the injection of contrast material (69 mL of iohexol; Omnipaque 300 mg, GE Healthcare, Mississauga, Ontario, Canada [iodine concentration, 4 mL/sec]) in the arterial and venous phases to detect and classify the endoleak by using recognized criteria (23). All CT angiograms were acquired with a 64–detector row scanner, with retrospective gating, a tube voltage of 120 kV, a collimation of 0.6 mm, and a pitch of 0.2. Reconstruction of 70% of the cardiac cycle was typically used for analysis. A bolus-tracking method was used to start the arterial phase, whereas images in the venous phase were acquired 10 seconds after the end of the arterial phase.

Macroscopic tissue slides.—After sacrifice, the aorta was perfused with 10% buffered formalin at 150 mm Hg for 1 hour before it was harvested and fixed in formalin for 24 hours. For correlation with CT and US images, axial macroscopic slices that included the intact tissue–stent-graft interface were prepared every 3 mm by using a cutting system (Exakt, Norderstedt, Germany).

Pathologic studies were reviewed by a biomedical engineer (S.L., with 15 years of experience in endovascular biomaterial research).

Characterization and segmentation of region of interest (endoleak, fresh thrombus, and organized thrombus).— On the basis of the craniocaudal level of the axial acquisitions, the maximum diameter of the aneurysm, and stent-graft orientation inside the aneurysm, registration between CT images, Doppler US images, macroscopic slices, and RF US images was performed after sacrifice. Endoleak areas were defined as areas with contrast enhancement at CT and a defect in the macroscopic slices. CT study interpretation and segmentation were performed independently by a graduate student (A.B.) with supervision by an experienced vascular radiologist (G.S.). The areas of organized and fresh thrombi were identified and delineated on macroscopic tissue slides after all information from the three techniques (digital subtraction angiography, CT, and B-mode and color Doppler US) was matched (Fig 2). A fresh thrombus was defined on macroscopic cuts as an area of loose thrombus with a black-brown coloration, which corresponded to a fibrin blood clot containing phantoms of red blood cells and no visible fibrous organization at histologic examination (Fig 3). Organized thrombus had a dense and yellowish appearance indicative of fibrous organization.

Once endoleaks and thrombi were identified, manual segmentations of the

endoleak area and the organized and fresh portions of thrombi were performed in all imaging modalities except RF US. An application developed by our team for carotid artery segmentation was adapted for the segmentation of regions of interest (endoleak, organized thrombus, and fresh thrombus) on RF images (24). All segmentations were performed by a graduate student (E.S.) supervised by the same vascular radiologist (G.S.). The NIVE-LSME method was applied to compute time-varying curves of axial strain averaged over segmented areas for three or more consecutive cardiac cycles (Fig 4) (25). NIVE analysis was performed by the same graduate student (E.S.) supervised by a biomedical engineer (G.C., with 20 years of experience in in vascular US). Figure 5 describes the protocol adopted for segmentation with each imaging modality.

Strain Parameters

Five NIVE strain parameters were investigated: the maximum and minimum axial strains, the maximum cumulative (MC) axial strain, and the maximum and minimum strain rates. Maximum axial strain and minimum axial strain represent the mean value, over acquired cardiac cycles, of positive and negative peaks of the time-varying instantaneous axial strain curve, respectively (Fig 4a). The maximum positive axial strain corresponds to the peak dilatation, whereas the minimum negative axial strain represents the peak compression of the tissue. MC axial strain is the average, over acquired cardiac cycles, of maximum positive values of the cumulated axial strain curve, corresponding to peak dilatation (Fig 4b). The last two parameters, defined as the speed of deformation during a cardiac cycle, were computed from the time derivative of the instantaneous filtered axial strain curve, as previously defined (25). Maximum strain rate represents the time-averaged positive peaks of the strain rate curve, whereas minimum strain rate represents the mean of the negative peaks.

Statistical Analysis

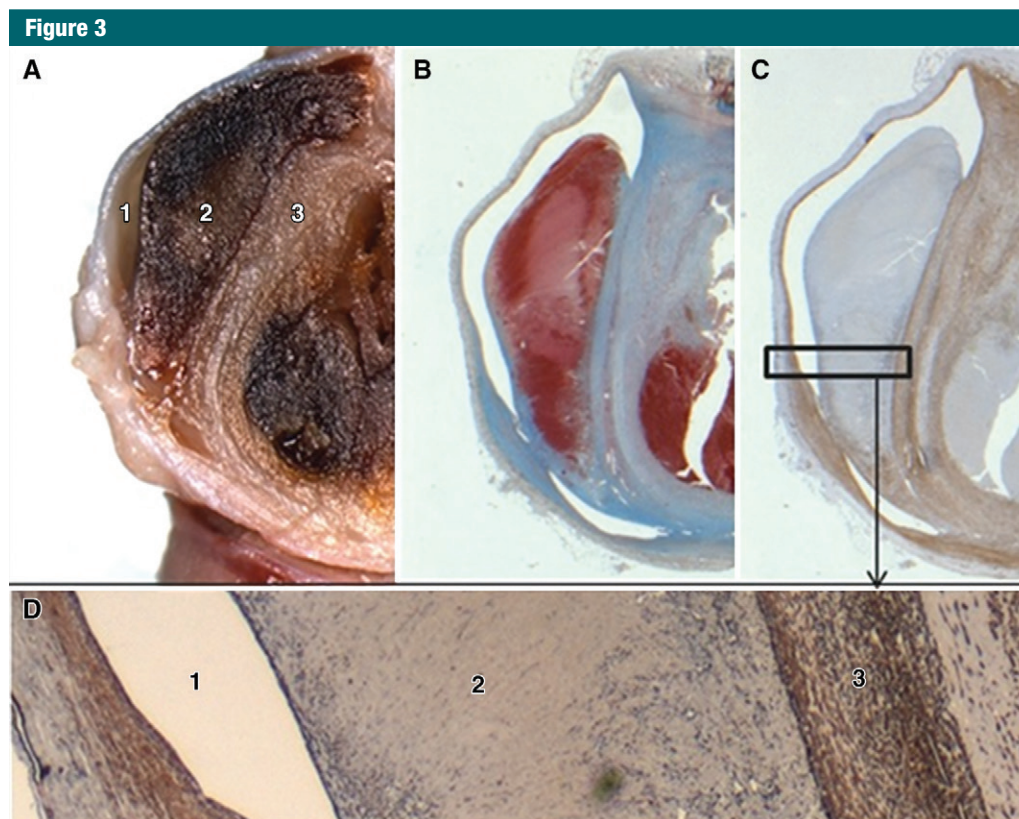Statistical tests were performed by using SigmaStat (version 3.11; Systat

Figure 3: *A,* Example macroscopic tissue slide shows endoleak *(1),* fresh thrombus *(2),* and organized thrombus *(3). B–D,* Corresponding histologic slides with, *B,* Movat staining and, *C,* and *D,* immunostaining of α–smooth muscle actin (brown). The brown regions correspond to dense fibrous connective tissues (organized thrombus). The blue regions correspond to fresh thrombus; the histologic slides thus confirm the areas of fresh thrombus (loose thrombus with black-brown coloration and absence of fibrous organization) and organized thrombus (areas of dense fibrous organization with a yellowish appearance) on the macroscopic slide.

Software, San Jose, Calif). Outcome comparisons of NIVE parameters (eg, maximum axial strain, minimum axial strain) between endoleak, organized thrombus, and fresh thrombus strain groups were analyzed by using the Kruskal-Wallis method. All two-by-two multiple comparisons were estimated by using the Wilcoxon rank-sum test, where statistical significance was adjusted with use of the Bonferroni correction. For each group (endoleak, organized thrombus, fresh thrombus), comparisons of strain results were performed between type I and II endoleaks by using the Wilcoxon rank-sum test.

For correlation between strain values, aneurysm sac systemic pressure measurements, endoleak area, and aneurysm size (maximal diameter and area) at sacrifice, Pearson correlation tests were performed. Statistical significance was set at $P < .05$. Data are presented as means ± standard deviations.

Results

Technical Success and Evolution of Endoleak

AAAs and stent-grafts were successfully created and implanted, respectively, in all animals. No complications occurred during the study. Four dogs had a type I endoleak (all from group 1), 13 dogs had a type II endoleak (one from group 1, seven from group 2, and five from group 3), and one dog (from group 3) had no endoleak and thus a perfect seal of the aneurysm sac. One type I endoleak converted

to a type II endoleak, probably because of inadequate undersizing of the stent-graft. Five EVARs aiming for a complete sealing eventually resulted in type II endoleaks, probably because of the presence of lumbar arteries that were not accessible for ligation. In total, all 18 dogs had solid thrombus in the sac; six of these dogs also had fresh thrombus. The mean maximum diameter of the AAAs was 20.7 mm ± 6.5.

As mentioned above, five NIVE strain parameters were investigated: Maximum and minimum axial strain, MC axial strain, and maximum and minimum strain rate (25). All five parameters showed significant differences ($P < .001$) when we compared results in areas that corresponded to an endoleak with those in areas that

Figure 4
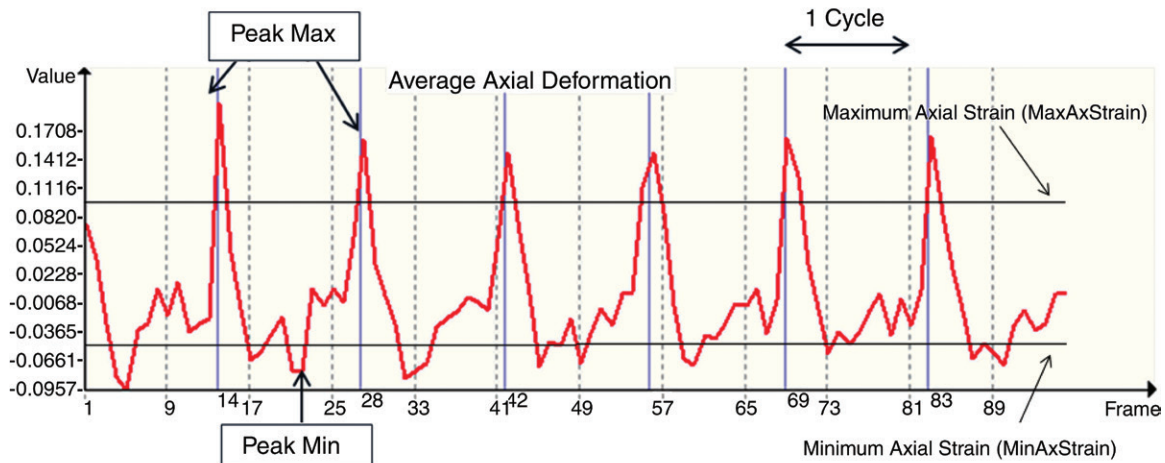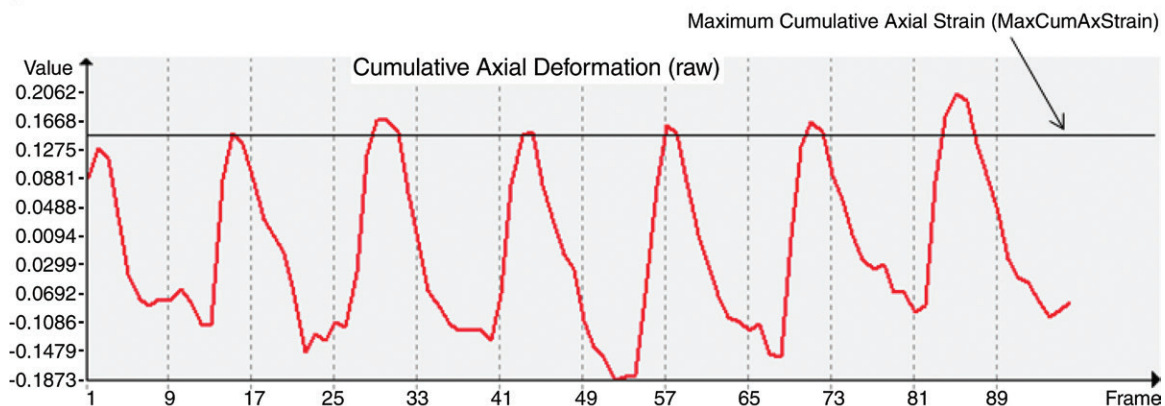
Figure 4: **(a)** LSME was applied to compute time-varying strain curves for three or more consecutive cardiac cycles. The instantaneous axial strain curve in 90 frames (seven cycles) is shown. Maximum axial strain and minimum axial strain represent the mean value, over acquired cardiac cycles, of positive and negative peaks of the time-varying instantaneous axial strain curve, respectively. **(b)** A cumulative axial strain curve over the same 90 frames (seven cycles). MC axial strain *(MaxCumAxStrain)* is the average, over acquired cardiac cycles, of maximum positive values of the cumulated axial strain curve, corresponding to peak dilatation. *Max* = maximum, *Min* = minimum.

corresponded to a solid or a fresh thrombus. Only the maximum axial strain and minimum strain rate parameters showed significant differences ($P < .001$) between solid and fresh thrombi (Table 1). Figure 6 reports differences for maximum axial strain.

Comparison between Type I and Type II Endoleaks

We further compared strain parameters for the three categories of aneurysmal sac tissue properties (endoleak, fresh thrombus, and organized thrombus) for

AAAs with type I endoleaks and those with type II endoleaks. As summarized in Table 2, all five strain parameters showed no statistically significant differences between the two endoleak groups.

Correlation between Strain, Sac Pressure, and Systemic Pressure Measurements

The mean sac pressure in AAAs with type I endoleaks and those with type II endoleaks were estimated at 67.5 mm Hg ± 20.6 and 51.9 mm Hg ± 19.8, respectively ($P = .2$). Because maximum axial strain and mean strain rate

could be used ot discriminate between aneurysmal sac tissue properties, those measures were correlated with mean pressure values within the sac, as well as systemic pressure. There were no significant correlations ($P > .05$) between any of these parameters.

Correlation between Strain Measurements and Aneurysm Size

Geometric measures (endoleak area and maximal aneurysm diameter and area) were correlated with strain parameters. No significant correlations were found ($P > .05$).
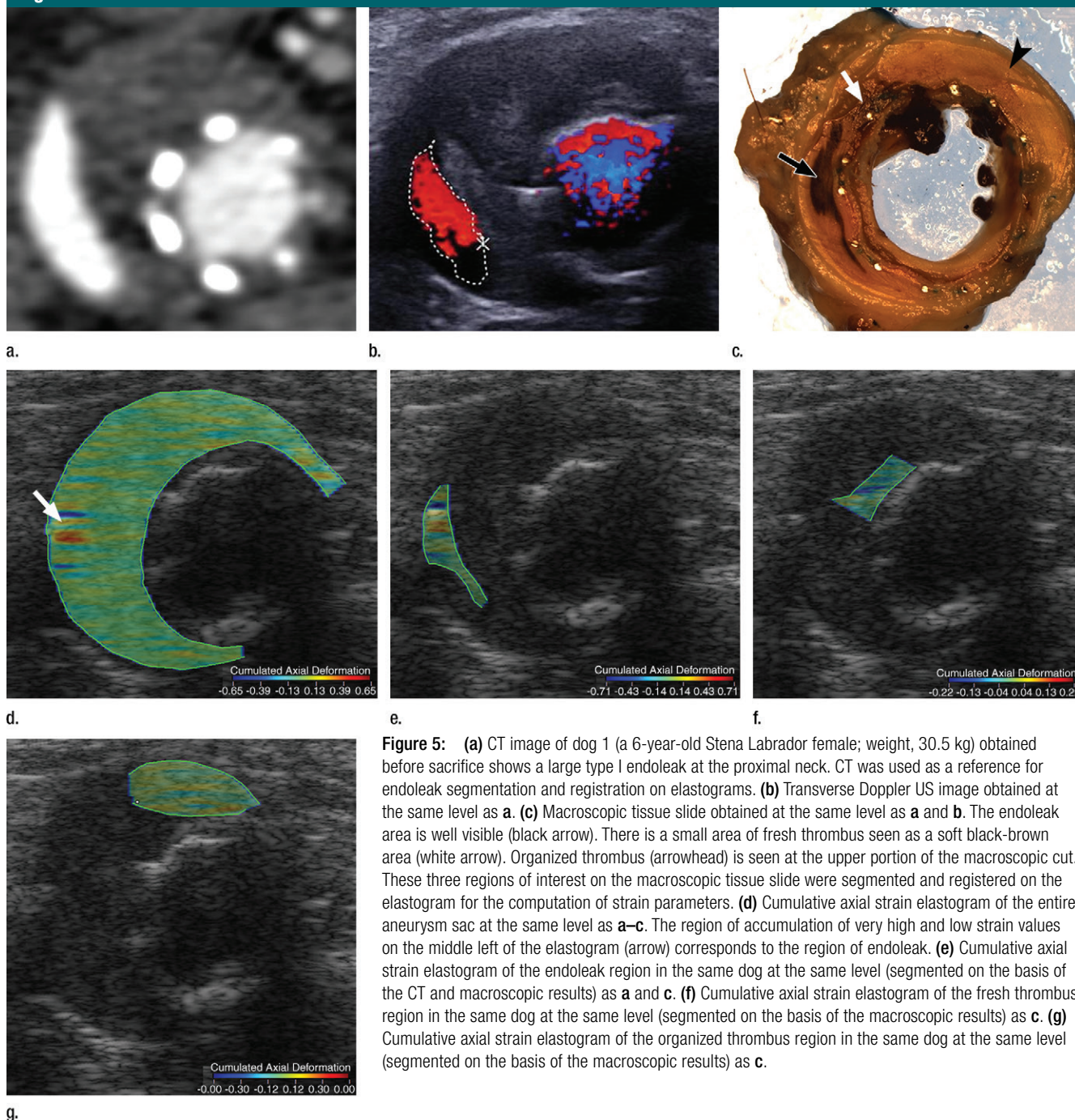
Figure 5

Figure 5: **(a)** CT image of dog 1 (a 6-year-old Stena Labrador female; weight, 30.5 kg) obtained before sacrifice shows a large type I endoleak at the proximal neck. CT was used as a reference for endoleak segmentation and registration on elastograms. **(b)** Transverse Doppler US image obtained at the same level as **a**. **(c)** Macroscopic tissue slide obtained at the same level as **a** and **b**. The endoleak area is well visible (black arrow). There is a small area of fresh thrombus seen as a soft black-brown area (white arrow). Organized thrombus (arrowhead) is seen at the upper portion of the macroscopic cut. These three regions of interest on the macroscopic tissue slide were segmented and registered on the elastogram for the computation of strain parameters. **(d)** Cumulative axial strain elastogram of the entire aneurysm sac at the same level as **a–c**. The region of accumulation of very high and low strain values on the middle left of the elastogram (arrow) corresponds to the region of endoleak. **(e)** Cumulative axial strain elastogram of the endoleak region in the same dog at the same level (segmented on the basis of the CT and macroscopic results) as **a** and **c**. **(f)** Cumulative axial strain elastogram of the fresh thrombus region in the same dog at the same level (segmented on the basis of the macroscopic results) as **c**. **(g)** Cumulative axial strain elastogram of the organized thrombus region in the same dog at the same level (segmented on the basis of the macroscopic results) as **c**.

Discussion

Evaluation of thrombus stiffness strain measurements with the NIVE technique could be valuable in assessing adequate AAA sac healing after EVAR. With this preclinical model, we could confirm the feasibility of NIVE for the characterization of endoleaks and thrombus organization after EVAR. The LSME algorithm estimated the strain transmitted by cardiac pulsation inside the aneurysm sac by computing axial and lateral strain and shear maps from RF US images (16–19). No external compression or radiation force was needed.

Our results showed that endoleak, organized thrombus, and fresh thrombus

Radiology

Table 1

NIVE Strain Parameters in Segmented Regions

Parameter (%)	Endoleak	Organized Thrombus	Fresh Thrombus	Endoleak vs Organized Thrombus	Endoleak vs Fresh Thrombus	Organized Thrombus vs Fresh Thrombus
				P Value*		
Maximum axial strain	0.78 ± 0.22	0.10 ± 0.04	0.23 ± 0.02	<.001	<.001	<.001
Minimum axial strain	−0.44 ± 0.30	−0.17 ± 0.06	−0.17 ± 0.05	.004	.023	.818
MC axial strain	0.85 ± 0.56	0.16 ± 0.10	0.20 ± 0.08	<.001	.002	.316
Maximum strain rate	5.61 ± 3.75	1.16 ± 0.60	1.66 ± 0.69	<.001	.006	.11
Minimum strain rate	−6.00 ± 3.71	−1.10 ± 0.53	−1.76 ± 0.81	<.001	.006	.033

* Calculated with the Wilcoxon rank-sum test.

areas display different strain values at NIVE. Thus, this technique could be capable of revealing an endoleak in addition to being able to help characterize the thrombus region. In this setting, NIVE could be used as a tool to monitor the healing process inside the aneurysm sac after EVAR (26). The high strain values observed within the endoleak area were due to the highly heterogeneous content inside the segmented region; it consisted of slow blood flow that induces some RF signal decorrelation mixed with immature soft thrombus that promotes high deformations (20). Signal decorrelation is due to the high signal variation in the same area. On the other hand, organized thrombus is a solid homogeneous tissue. This stiffer tissue expresses lower strain values and rates of deformation when subjected to blood pulsation. Fresh thrombi, regions of immature structuring, displayed lower strain values than solid thrombi and higher strain values than endoleaks. Reported strain results may be used to identify specific aneurysm regions and possibly follow aneurysm healing with time (27–29). Indeed, characterization of thrombus organization has been presented as a new concept of follow-up with MR imaging (30,31). It has been shown that thrombus intensity at MR imaging inside the aneurysm sac can be used for the detection of endotension and AAA growth (30,32). However, MR imaging has limited accessibility and higher cost than US, and MR images are degraded by metal artifacts when stainless-steel stent-graft are used (33).

This seems to be an opportunity for use of the NIVE-LSME method in characterizing aneurysm sacs. We believe that in a clinical workflow, NIVE data could be easily acquired at the end of a complete B-mode and color Doppler examination to characterize thrombus organization and possibly depict slow-flow endoleaks that cannot be seen with routine Doppler examination (10,14,15).

Differences in strain values could be expected when comparing aneurysms with type I and II endoleaks. Indeed, those endoleaks generally have different sac pressure measurements, as type I endoleaks are typically at systemic pressure, whereas retrograde flow in type II endoleaks has lower pressure (34–36). An unexpected observation was the independence of strain results from sac pressure. There was no correlation between the pressure measured inside the aneurysm sac and strain values for the endoleak, organized thrombus, and fresh thrombus areas. This may be explained by the fact that strain was measured between two consecutive RF images at different pressures (37). It is thus mainly influenced by the systolic and diastolic amplitude range and less by the mean pressure. Because most biologic tissues display nonlinear stress-strain relationships, mean pressure is, to a lesser extent, a potential cofounding factor that should be considered. Note that we could not measure the pulse pressure amplitude within the aneurysm sacs with available pressure sensors.

It is logical to observe larger endoleak areas in larger aneurysms (38). However,
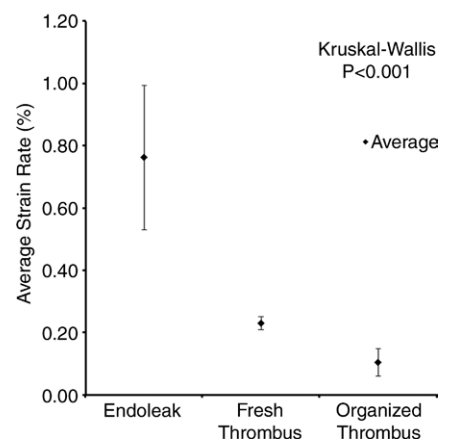
Figure 6

Figure 6: Graph shows mean maximum axial strain values and standard deviations for the three regions of interest. There was a significant difference (*P* < .01) in mean maximum axial strain between endoleak, organized thrombi, and fresh thrombi.

leak size had no impact on strain measurements, which is an intrinsic property of the tissue being examined.

The main limitation of our study was its design, which was based on a validation of strain values for the three AAA components (endoleaks, organized thrombi, and fresh thrombi). This validation was performed after the registration of our regions of interest on the basis of CT and macroscopic findings on the NIVE acquisitions. Because elastograms were not displayed in real time (they required 5 minutes postprocessing time), the operator was not able to have visual feedback on strain values during image acquisition.

Table 2

Comparison of Strain Values in Endoleak, Organized Thrombus, and Fresh Thrombus Regions as a Function of Endoleak Type

Parameter and Region	Type I Endoleak	Type II Endoleak	P Value
Maximum axial strain (%)			
Endoleak	0.87 ± 0.34	0.74 ± 0.21	.39
Organized thrombus	0.10 ± 0.03	0.10 ± 0.04	.93
Fresh thrombus	0.25	0.23 ± 0.02	NA
Minimum axial strain (%)			
Endoleak	−0.68 ± 0.32	−0.47 ± 0.40	.41
Organized thrombus	−0.19638 ± 0.07	−0.17 ± 0.06	.49
Fresh thrombus	−0.16	−0.17 ± 0.05	NA
MC axial strain (%)			
Endoleak	0.96 ± 0.54	0.83 ± 0.56	.72
Organized thrombus	0.19 ± 0.09	0.15 ± 0.09	.46
Fresh thrombus	0.30	0.19 ± 0.08	NA
Maximum strain rate (%)			
Endoleak	6.55 ± 3.74	5.55 ± 3.77	.68
Organized thrombus	1.10 ± 0.21	1.18 ± 0.69	.95
Fresh thrombus	1.35	1.72 ± 0.75	NA
Minimum strain rate (%)			
Endoleak	−8.77 ± 5.17	−5.38 ± 3.10	.14
Organized thrombus	−1.23 ± 0.42	−1.06 ± 0.57	.59
Fresh thrombus	−1.40	−1.82 ± 0.89	NA

Note.—No significant difference was found for any of the parameters. NA = not applicable.

In this setting, it was not possible to compare directly the diagnostic accuracy of elastography with that of Doppler US or CT. Furthermore, to enable detection of endoleaks or thrombus characteristics, diagnostic thresholds would need to be defined. Therefore, we cannot make conclusions regarding the clinical impact of the technique. In our study, we were able to set a mean strain percentage and standard deviation for the different regions of interest (endoleak, fresh thrombus, and organized thrombus). We will use these values to set optimal thresholds in our future clinical study to evaluate the clinical accuracy of NIVE (39).

Our model also did not reproduce the biologic environment of atherosclerotic AAA nor the weakening of the aortic wall. However, it reproduced accurately the hemodynamic and physiologic environment of failed or successful EVARs because we could preserve or not the collateral circulation and vary the seal on stent-graft landing zones. Thus, we believe, it is appropriate for the study of endoleak and thrombus organization. Moreover, in our study, we did not analyze the strain of the AAA wall and focused on the analysis of sac content.

Practical applications: Our results show that different values of NIVE parameters were displayed in endoleak and in thrombi with different grades of organization inside the aneurysm sac. Even though NIVE could not help differentiate type I and II endoleaks, it could be a good addition to the radiology arsenal for characterizing thrombus organization and slow-flow endoleaks not seen at Doppler US and CT and reduce the need for CT angiography during EVAR follow-up.

References

1. Greenhalgh RM, Brown LC, Kwong GP, Powell JT, Thompson SG; EVAR trial participants. Comparison of endovascular aneurysm repair with open repair in patients with abdominal aortic aneurysm (EVAR trial 1), 30-day operative mortality results: randomised controlled trial. Lancet 2004;364(9437): 843–848.

2. Prinssen M, Verhoeven EL, Buth J, et al. A randomized trial comparing conventional and endovascular repair of abdominal aortic aneurysms. N Engl J Med 2004;351(16): 1607–1618.

3. EVAR trial participants. Endovascular aneurysm repair versus open repair in patients with abdominal aortic aneurysm (EVAR trial 1): randomised controlled trial. Lancet 2005; 365(9478):2179–2186.

4. Blankensteijn JD, de Jong SE, Prinssen M, et al. Two-year outcomes after conventional or endovascular repair of abdominal aortic aneurysms. N Engl J Med 2005;352(23): 2398–2405.

5. Tadros RO, Faries PL, Ellozy SH, et al. The impact of stent graft evolution on the results of endovascular abdominal aortic aneurysm repair. J Vasc Surg 2014;59(6):1518–1527 .

6. Nordon IM, Karthikesalingam A, Hinchliffe RJ, Holt PJ, Loftus IM, Thompson MM. Secondary interventions following endovascular aneurysm repair (EVAR) and the enduring value of graft surveillance. Eur J Vasc Endovasc Surg 2010;39(5):547–554.

7. Dill-Macky MJ, Wilson SR, Sternbach Y, Kachura J, Lindsay T. Detecting endoleaks in aortic endografts using contrast-enhanced sonography. AJR Am J Roentgenol 2007; 188(3):W262–W268.

8. Brown LC, Brown EA, Greenhalgh RM, Powell JT, Thompson SG; UK EVAR Trial Participants. Renal function and abdominal aortic aneurysm (AAA): the impact of different management strategies on long-term renal function in the UK EndoVascular Aneurysm Repair (EVAR) Trials. Ann Surg 2010;251(5):966–975.

9. Prinssen M, Wixon CL, Buskens E, Blankensteijn JD. Surveillance after endovascular an-

eurysm repair: diagnostics, complications, and associated costs. Ann Vasc Surg 2004; 18(4):421–427.

10. Sun Z. Diagnostic value of color duplex ultrasonography in the follow-up of endovascular repair of abdominal aortic aneurysm. J Vasc Interv Radiol 2006;17(5):759–764.

11. Beeman BR, Doctor LM, Doerr K, McAfee-Bennett S, Dougherty MJ, Calligaro KD. Duplex ultrasound imaging alone is sufficient for midterm endovascular aneurysm repair surveillance: a cost analysis study and prospective comparison with computed tomography scan. J Vasc Surg 2009;50(5):1019–1024.

12. Go MR, Barbato JE, Rhee RY, Makaroun MS. What is the clinical utility of a 6-month computed tomography in the follow-up of endovascular aneurysm repair patients? J Vasc Surg 2008;47(6):1181–1186; discussion 1186–1187.

13. Sternbergh WC 3rd, Greenberg RK, Chuter TA, Tonnessen BH; Zenith Investigators. Redefining postoperative surveillance after endovascular aneurysm repair: recommendations based on 5-year follow-up in the US Zenith multicenter trial. J Vasc Surg 2008; 48(2):278–284; discussion 284–285.

14. AbuRahma AF, Welch CA, Mullins BB, Dyer B. Computed tomography versus color duplex ultrasound for surveillance of abdominal aortic stent-grafts. J Endovasc Ther 2005;12(5): 568–573.

15. Elkouri S, Panneton JM, Andrews JC, et al. Computed tomography and ultrasound in follow-up of patients after endovascular repair of abdominal aortic aneurysm. Ann Vasc Surg 2004;18(3):271–279.

16. Maurice RL, Ohayon J, Finet G, Cloutier G. Adapting the Lagrangian speckle model estimator for endovascular elastography: theory and validation with simulated radio-frequency data. J Acoust Soc Am 2004;116(2): 1276–1286.

17. Maurice RL, Fromageau J, Cardinal MH, et al. Characterization of atherosclerotic plaques and mural thrombi with intravascular ultrasound elastography: a potential method evaluated in an aortic rabbit model and a human coronary artery. IEEE Trans Inf Technol Biomed 2008;12(3):290–298.

18. Schmitt C, Soulez G, Maurice RL, Giroux MF, Cloutier G. Noninvasive vascular elastography: toward a complementary characterization tool of atherosclerosis in carotid arteries. Ultrasound Med Biol 2007;33(12): 1841–1858.

19. Naim C, Cloutier G, Mercure E, et al. Characterisation of carotid plaques with ultrasound elastography: feasibility and correlation with high-resolution magnetic resonance imaging. Eur Radiol 2013;23(7):2030–2041.

20. Fromageau J, Lerouge S, Maurice RL, Soulez G, Cloutier G. Noninvasive vascular ultrasound elastography applied to the characterization of experimental aneurysms and follow-up after endovascular repair. Phys Med Biol 2008;53(22):6475–6490.

21. Lerouge S, Raymond J, Salazkin I, et al. Endovascular aortic aneurysm repair with stent-grafts: experimental models can reproduce endoleaks. J Vasc Interv Radiol 2004;15(9): 971–979.

22. Soulez G, Lerouge S, Salazkin I, Darsaut T, Oliva VL, Raymond J. Type I and collateral flow in experimental aneurysm models treated with stent-grafts. J Vasc Interv Radiol 2007;18(2):265–272.

23. Stavropoulos SW, Charagundla SR. Imaging techniques for detection and management of endoleaks after endovascular aortic aneurysm repair. Radiology 2007;243(3):641–655.

24. Destrempes F, Meunier J, Giroux MF, Soulez G, Cloutier G. Segmentation of plaques in sequences of ultrasonic B-mode images of carotid arteries based on motion estimation and a Bayesian model. IEEE Trans Biomed Eng 2011;58(8).

25. Mercure E, Destrempes F, Roy Cardinal MH, et al. A local angle compensation method based on kinematics constraints for non-invasive vascular axial strain computations on human carotid arteries. Comput Med Imaging Graph 2014;38(2):123–136.

26. Kulcsár Z, Houdart E, Bonafé A, et al. Intra-aneurysmal thrombosis as a possible cause of delayed aneurysm rupture after flow-diversion treatment. AJNR Am J Neuroradiol 2011;32(1):20–25.

27. Ashton JH, Vande Geest JP, Simon BR, Haskett DG. Compressive mechanical properties of the intraluminal thrombus in abdominal aortic aneurysms and fibrin-based thrombus mimics. J Biomech 2009;42(3):197–201.

28. Wang DH, Makaroun M, Webster MW, Vorp DA. Mechanical properties and microstructure of intraluminal thrombus from abdominal aortic aneurysm. J Biomech Eng 2001;123(6):536–539.

29. Gasser TC, Görgülü G, Folkesson M, Swedenborg J. Failure properties of intraluminal thrombus in abdominal aortic aneurysm under static and pulsating mechanical loads. J Vasc Surg 2008;48(1):179–188.

30. Cornelissen SA, van der Laan MJ, Vincken KL, et al. Use of multispectral MRI to monitor aneurysm sac contents after endovascular abdominal aortic aneurysm repair. J Endovasc Ther 2011;18(3):274–279.

31. Engellau L, Larsson EM, Albrechtsson U, et al. Magnetic resonance imaging and MR angiography of endoluminally treated abdominal aortic aneurysms. Eur J Vasc Endovasc Surg 1998;15(3):212–219.

32. Nguyen VL, Leiner T, Hellenthal FA, et al. Abdominal aortic aneurysms with high thrombus signal intensity on magnetic resonance imaging are associated with high growth rate. Eur J Vasc Endovasc Surg 2014;48(6): 676–684.

33. Weigel S, Tombach B, Maintz D, et al. Thoracic aortic stent graft: comparison of contrast-enhanced MR angiography and CT angiography in the follow-up: initial results. Eur Radiol 2003;13(7):1628–1634.

34. Dayal R, Mousa A, Bernheim J, et al. Characterization of retrograde collateral (type II) endoleak using a new canine model. J Vasc Surg 2004;40(5):985–994.

35. Dias NV, Ivancev K, Malina M, Resch T, Lindblad B, Sonesson B. Intra-aneurysm sac pressure measurements after endovascular aneurysm repair: differences between shrinking, unchanged, and expanding aneurysms with and without endoleaks. J Vasc Surg 2004;39(6):1229–1235.

36. Dias NV, Ivancev K, Resch TA, Malina M, Sonesson B. Endoleaks after endovascular aneurysm repair lead to nonuniform intra-aneurysm sac pressure. J Vasc Surg 2007;46(2): 197–203.

37. Maurice RL, Ohayon J, Frétigny Y, Bertrand M, Soulez G, Cloutier G. Noninvasive vascular elastography: theoretical framework. IEEE Trans Med Imaging 2004;23(2):164–180.

38. Ellozy SH, Carroccio A, Lookstein RA, et al. Abdominal aortic aneurysm sac shrinkage after endovascular aneurysm repair: correlation with chronic sac pressure measurement. J Vasc Surg 2006;43(1):2–7.

39. Centre Hospitalier de l'Université de Montréal (CHUM). Abdominal Aortic Aneurysm Follow-up After Endovascular Repair by Non-invasive Vascular Elastography. Clinicaltrials.gov. http://clinicaltrials.gov/ct2/show/NCT01907386?term=abdominal+aortic+aneurysm&recr=Not+yet+recruiting&rslt=Without&type=Intr&titles=abdominal+aortic+aneurysm+follow-up+after+endovascular+repair+by+non-invasive+vascular+elastography&cntry1=NA%3ACA&state1=NA%3ACA%3AQC&locn=Montreal&rank=1. Last updated October 29, 2013. Accessed December 9, 2015.